



Article

Direct Epoxidation of Hexafluoropropene Using Molecular Oxygen over Cu-Impregnated HZSM-5 Zeolites

Jie-Ming Huang ^{1,2}, Jingning Guo ³, Chengmiao Xu ³, An Su ^{4,*} , Ke-Jun Wu ^{1,2,*} and Chao-Hong He ^{1,2} ¹ Zhejiang Provincial Key Laboratory of Advanced Chemical Engineering Manufacture Technology, College of Chemical and Biological Engineering, Zhejiang University, Hangzhou 310027, China² Institute of Zhejiang University-Quzhou, Quzhou 324000, China³ Zhejiang Anglikang Pharmaceutical Co., Ltd., Shaoxing 312400, China⁴ State Key Laboratory Breeding Base of Green Chemistry-Synthesis Technology, Key Laboratory of Green Chemistry-Synthesis Technology of Zhejiang Province, College of Chemical Engineering, Zhejiang University of Technology, Hangzhou 310014, China

* Correspondence: ansu@zjut.edu.cn (A.S.); k.wu@zju.edu.cn (K.-J.W.)

Abstract: This study explores a novel method of directly epoxidizing hexafluoropropene with molecular oxygen under gaseous conditions using a Cu/HZSM-5 catalytic system (Cu/HZ). An in-depth investigation was conducted on the catalytic performance of Cu-based catalysts on various supports and Cu/HZ catalysts prepared under different conditions. Cu/HZ catalysts exhibited better catalytic performance than other porous medium-supported Cu catalysts for the epoxidation of hexafluoropropene by molecular oxygen. The highest propylene oxide yield of 35.6% was achieved over the Cu/HZ catalyst prepared under conditions of 350 °C with a Cu loading of 1 wt%. By applying characterization techniques including XRD, BET, NH₃-TPD, and XPS to different catalyst samples, the relationship between the interaction of Cu²⁺ and HZSM-5 and the reactivity of the catalyst was studied, thereby elucidating the influence of calcination temperature and loading on the reactivity. Finally, we further proposed the possible mechanism of how isolated Cu²⁺ and acid sites improve catalytic performance.

Keywords: epoxidation; modified HZSM-5; hexafluoropropene; hexafluoropropylene oxide



Citation: Huang, J.-M.; Guo, J.; Xu, C.; Su, A.; Wu, K.-J.; He, C.-H. Direct Epoxidation of Hexafluoropropene Using Molecular Oxygen over Cu-Impregnated HZSM-5 Zeolites. *Processes* **2024**, *12*, 1520. <https://doi.org/10.3390/pr12071520>

Academic Editor: Wladimir Reschetilowski

Received: 18 June 2024

Revised: 12 July 2024

Accepted: 16 July 2024

Published: 19 July 2024



Copyright: © 2024 by the authors. Licensee MDPI, Basel, Switzerland. This article is an open access article distributed under the terms and conditions of the Creative Commons Attribution (CC BY) license (<https://creativecommons.org/licenses/by/4.0/>).

1. Introduction

Hexafluoropropylene oxide (HFPO), as an important intermediate in the fluorine chemical industry, has high commercial value and is widely used in synthesizing drugs and fluoropolymers [1]. Presently, HFPO is chiefly synthesized through the epoxidation reaction of hexafluoropropene (HFP). The early synthesis methods using nucleophiles, such as sodium hypochlorite and hydrogen peroxide, are gradually being used less because of the environmental problems caused by the reaction's wastewater [2–5]. Currently, the main industrial method for producing hexafluoropropene oxide is oxygenating hexafluoropropene with molecular oxygen in liquid phase. However, this liquid-phase method operates under high pressure and demands sophisticated equipment, making continuous preparation challenging. In contrast to the liquid-phase method, gaseous-phase direct epoxidation of HFP by molecular oxygen into HFPO, due to its clean and simple reaction system, is a potentially fruitful area of research.

In recent years, catalysts based on silver [6,7], copper [8,9], barium [10], cobalt [11], and other metals, mainly supported on porous substances (e.g., Al₂O₃ and silica gel), have been investigated for gaseous-phase epoxidation of HFP. Huang et al. proposed a silver catalytic system directly oxygenating hexafluoropropene with molecular oxygen, and the Ag/ γ -Al₂O₃ catalyst they prepared achieved a selectivity of up to 41.1% but a yield of HFPO of only 5.06%, while adding Cs improved the selectivity and yield to 16.5% and 7.89%, respectively [6]. Lokhat et al. designed a copper-coiled tube reactor and performed

catalyst-free production of HFPO under gaseous conditions, achieving conversion of up to 70% and a 40% yield at the cost of a reactor length of up to 115 m [12,13]. They further designed a kinetic model containing one primary reaction and seven secondary reactions to estimate the degree of reversibility of the individual reaction steps in the copper-coiled tube reactor [12–14]. As early as 1997, Oda et al. proposed the application of a Cu/SiO₂ system in epoxidation of HFP [8]. Subsequently, Ndlovu et al. introduced a Cs-doping strategy, which elevated the conversion rate and selectivity to 35.5% and 51.4%, respectively [9]. Despite overcoming some of the drawbacks of the liquid-phase reaction, the catalytic system for gaseous-phase epoxidation of HFP still leaves considerable room for improvement.

ZSM-5 zeolites are silico-aluminate porous materials with an MFI structure constructed of eight five-membered rings [15]. ZSM-5 has been widely used as a support in catalytic fields due to its excellent porous structure, controllable acidity, stable structure, and large surface area [16,17]. ZSM-5 zeolites loaded with Cu have been explored as key catalysts for oxidating methane to methanol [18]. Therefore, the capacity of modified ZSM-5 in the selective oxidation of other low-molecular-weight compounds warrants anticipation. Moreover, the cations in ZSM-5 can be replaced with H⁺ by ion exchange and calcination to obtain HZSM-5, which inherits the pore structure of ZSM-5 and has more acidic sites than ZSM-5. It makes HZSM-5 even more suitable for oxidation reaction.

The epoxidation reaction is a partial oxidation. As a result, the catalytic activity of the catalyst should be more stringently controlled, and it cannot be too high or too low. Moreover, studies have demonstrated the potential of transition metal oxides supported on zeolite catalysts in the epoxidation of propylene [19–21]. As a common transition metal, Cu has a variety of chemical states, which can meet the complex needs of epoxidation reactions for catalysts. At the same time, Cu is easily available in nature to meet the needs of industrial production and Cu has been found to have epoxidation properties in previous studies [22]. Unlike Ag, which needs a temperature above 200 °C for epoxidation [23], Cu could work at lower temperatures. Since HFPO begins decomposing at around 160 °C, a Cu-based catalyst is expected to perform better for HFP epoxidation. Although Cu has so many advantages as a catalyst for epoxidation reaction, the reaction effect of Cu on the epoxidation of HFP is not outstanding. In view of this phenomenon, this article posits that the primary reason for the inability to further enhance the epoxidation of HFP with a Cu catalyst is due to support limitations. Based on this understanding, this study takes a novel approach to improve catalytic performance of the Cu-based system with emphasis on the support.

In this work, dispersing Cu species with epoxidation activity into the HZSM-5 zeolite system aims to enhance the performance of the epoxidation. Although an HZSM-5 zeolite catalyst has not been used for epoxidation before, its abundant acidic sites, stable structure, and large specific surface area are exactly the properties required for HFP epoxidation catalyst supports. The Cu supported on HZSM-5 zeolite was prepared via the impregnation method, which can meet many industrial application requirements. This is mainly because the impregnation method can better reduce the cost and time of catalyst preparation in industrial applications. To demonstrate the catalytic performance, the test results of a Cu-supported HZSM-5 zeolite catalyst were compared with those of other supports. By means of characterizations, the state of the Cu and the acidic sites of HZSM-5 were investigated to interpret the improvement of the catalytic system.

2. Experimental Section

2.1. Catalyst Preparation

Cu/HZSM-5 (Cu/HZ) catalysts with varied Cu content were prepared by the impregnation method. ZSM-5 (Si/Al = 38, H-type) was purchased from Xianfeng Nanomaterial Technology Co., Ltd. (Nan-jing China). The typical preparation procedure is to fully dissolve a certain amount of Cu(NO₃)₂ (Macklin Biochemical Co., Ltd., Shanghai, China) in deionized water, mix the carrier with the solution, and intensively stir for 3 h at room temperature. Stirring continues at 60 °C to remove water, and then the remaining solid is dried

at 60 °C for 2 h. The obtained solids are calcined for 5 h at a specified temperature, with a heating rate of 10 °C/min. The as-prepared catalyst is denoted as Cu_x/HZ-y, indicating catalysts at a Cu loading amount of x wt% calcined at the temperature of y °C.

When SiO₂ and Al₂O₃ act as supports, the impregnation, drying, and calcination conditions of the catalyst align with those of Cu/HZ. The catalysts supported on different supports are labeled as Cu/Al₂O₃, Cu/SiO₂. When acidified SiO₂ is employed as the carrier, it needs to be added to a solution of 1M HCl and vigorously stirred for 3 h before impregnation. The filtered-out SiO₂ is then washed with deionized water until the filtrate shows a neutral pH. After having been placed in a drying oven at 60 °C overnight, the acidified SiO₂ is obtained. The following impregnation, drying, and calcination conditions are consistent with Cu/HZ. The as-prepared catalyst is labelled as Cu/acid-SiO₂.

2.2. Catalyst Characterization

The microscopic structure of the catalyst was studied using transmission electron microscopy (TEM). The TEM tests were conducted on a Tecnai F30 (FEI, Eindhoven, The Netherlands). XRD (X-ray Diffraction) patterns were taken on an Empyrean 200,895 (PANalytical BV, Almelo, The Netherlands) diffractometer using Cu K α radiation, generating voltage 40 kV, tube current 40 mA, scanning range from 5° to 80°, step size 0.026°, and scanning speed 2°/min.

N₂ adsorption–desorption isotherms were obtained on ASAP 2460 (Micromeritics, Norcross, GA, USA) gas adsorption equipment at 77 K. Prior to the measurement, the sample was degassed at 300 °C for 6 h. The specific surface area was calculated according to the Brunauer–Emmert–Teller (BET) model. Elemental analysis was undertaken by Inductively Coupled Plasma Optical Emission Spectrometer (ICP-OES) using an Agilent 730 (OES) instrument (Agilent, Santa Clara, CA, USA) after complete dissolution of the sample in concentrated nitric acid.

The composite and oxidation states of the catalyst were determined by X-ray photoelectron spectroscopy. XPS spectra were recorded on an Escalab 250Xi (Perkin Elmer, Shelton, CT, USA) using Al K α ($h\nu = 1486.8$ eV) as the X-ray source. The C1s (binding energy at 284.8 eV) was used as the reference for charge correction.

H₂ temperature-programmed reduction (H₂-TPR) experiments were performed on a BELCat II (Microtrac, Osaka, Japan). Accurate amounts of the prepared samples (30–40 mg) were loaded into a U-shaped quartz tube, heated at a rate of 10 °C/min from room temperature to 120 °C for pre-dry-treatment, purged with He gas flow (50 mL/min) for 1 h, cooled to 50 °C, and then subject to inlet of a 10% H₂/Ar (50 mL/min) mixed-gas stream for 0.5 h. Once the baseline was stable, the sample was heated to 800 °C at 10 °C/min in a 10% H₂/Ar gas stream for desorption, and the reduced gas was detected by a TCD.

NH₃ temperature-programmed desorption (NH₃-TPD) required 80 mg of the sample to be placed in the reaction tube. The sample was heated at 10 °C/min in a He stream from room temperature to 260 °C for pre-dry-treatment. The He stream (30–50 mL/min) continued for 1 h, cooled to 50 °C, and a 10% NH₃/He (30–50 mL/min) mixed gas was introduced for 1 h to saturation. The He gas stream (30–50 mL/min) was switched and purged for 1 h to remove the weakly physically adsorbed NH₃. Finally, the sample was heated to 800 °C under a He atmosphere at a rate of 10 °C/min for desorption, and the desorbed gas was detected by TCD.

EPR (electron paramagnetic resonance) spectra of the samples were recorded using a EMXplus-6/1 (Bruker, Bremen, Germany) spectrometer to identify isolated Cu²⁺. The EPR spectra were recorded at room temperature and atmospheric pressure.

Thermogravimetric analysis (TG) experiments for catalyst samples were performed in a STA 449 F3 (Netzsch, Hanau, Germany). The sample was heated at a rate of 10 °C/min from room temperature to 800 °C under air atmosphere and the weight of the sample as it changed with temperature was recorded.

2.3. Catalytic Activity Test

The continuous epoxidation experiment of HFP was carried out on a pre-designed fixed bed, as shown in Figure 1. The catalytic activity of the catalyst samples for the epoxidation of HFP was measured through this reactor. The reactor consisted of a stainless-steel tube (50 cm long, 1 cm inner diameter) installed in an aluminum heating jacket. The reaction gas was a mixture of HFP and O₂, and all gas flows were controlled by mass flow controllers (ACU20FD-LC, Beijing Accurate Technology Co., Beijing, China), controlling the feed ratio to 2:1 and maintaining a total flow rate of 5 sccm. A total of 10 g of the catalyst was placed in the constant-temperature section of the fixed bed and slowly introduced into the mixed gases of HFP and O₂, in a ratio of 4:1, with pressure controlled to 0.3–0.4 Mpa and the sample then heated to 250 °C for activation. After the activation temperature had been reached, this was retained for three hours under the raw-material atmosphere. Then, the mass flow controller was adjusted to control the HFP and O₂ feed ratio and adjusted to the reaction temperature for reaction.

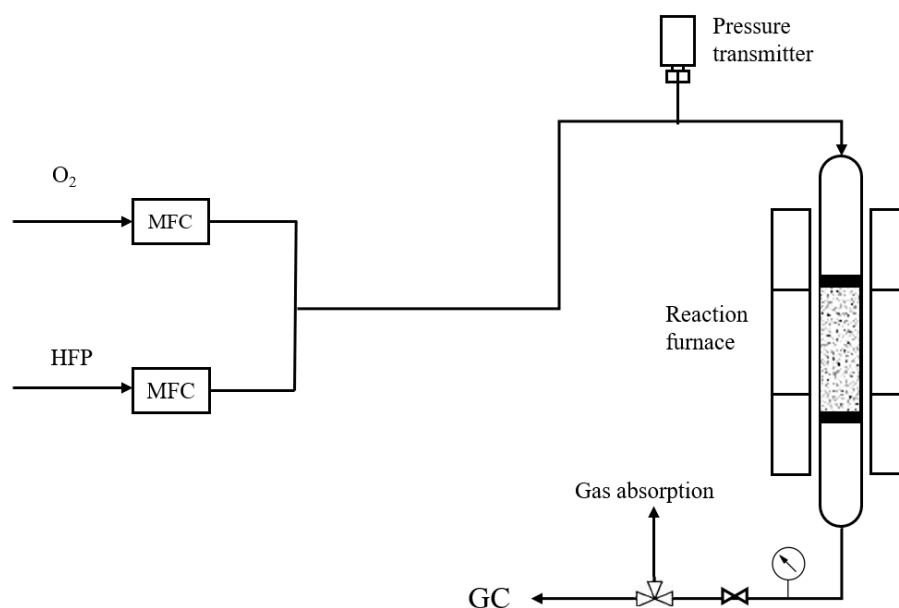


Figure 1. Diagram of the reactor designed for epoxidation of HFP.

Once the reactor temperature and pressure were stable, the composition was analyzed by a gas chromatograph (GC1690, Hangzhou JieDao Tech Co., Hangzhou, China) with an FID detector in the tail section, measuring the concentration of HFPO and HFP and calculating the conversion and selectivity of the reaction. In all experiments, due to the similar physical properties of the raw-material HFP and the target-product HFPO, it was difficult to separate the two on a conventional polysiloxane gas chromatography column, so a PoraBond Q (purchased from Agilent) in the PLOT column suitable for gaseous compound separation was used for analysis. Therefore, the HFP conversion and selectivity calculation equations are shown in Equations (1) and (2). Yield is obtained by multiplying conversion and selectivity.

$$X(\text{HFP}) = \frac{\text{HFP}_{\text{in}} - \text{HFP}_{\text{out}}}{\text{HFP}_{\text{in}}} \times 100\% \quad (1)$$

$$S(\text{HFPO}) = \frac{\text{HFPO} \times \alpha}{\text{HFP}_{\text{in}} - \text{HFP}_{\text{out}}} \times 100\% \quad (2)$$

where α is the correction factor for HFPO to HFP and the value is 5, which can be obtained through our preliminary measurement. See Figures S1 and S2 in Supplementary Materials for details. HFPO, HFP_{in}, and HFP_{out} are gas-phase peak areas, which were obtained by integrating the gas-phase chromatogram before and after the gas.

To better study the effect of different supports on the catalytic performance of the reaction, SiO_2 and Al_2O_3 were introduced as supports of the catalysts to compare their performance with HZSM-5. Considering that different carrier catalysts may have different most-suitable reaction temperatures, each different carrier catalyst was tested in a certain temperature range (160~220 °C), and other conditions remained unchanged to obtain the conversion and selection of the reaction at the most suitable temperature.

3. Results and Discussion

3.1. Characterization Results of the Prepared Catalyst

Cu/HZ catalysts calcinated at different temperatures were characterized by XRD for their crystallographic structure. As shown in Figure 2, all the samples exhibited characteristic peaks with 2θ at 7.9° , 8.8° , 23.1° , and 23.3° , corresponding to (101), (020), (332), and (051) facets of HZSM-5, respectively, which are the major phases in the pattern. This evidence indicates that HZSM-5 remains unchanged after undergoing the impregnation and calcination processes, maintaining the inherent MFI structure of HZSM-5. Perplexingly, at any calcination temperature, no noticeable peaks corresponded to Cu oxide on the XRD patterns of 1 wt%Cu/HZSM-5 (Cu_1/HZ) and 1 wt%Cu/HZSM-5 (Cu_5/HZ). This situation has also been reported in other studies related to copper catalysts [24]. The absence of diffraction peaks for CuO in the XRD spectra implies that these CuO microcrystals are too small or that the copper species are well dispersed on the surface of catalyst samples when loaded at low weights, preventing characterization of Cu species via XRD.

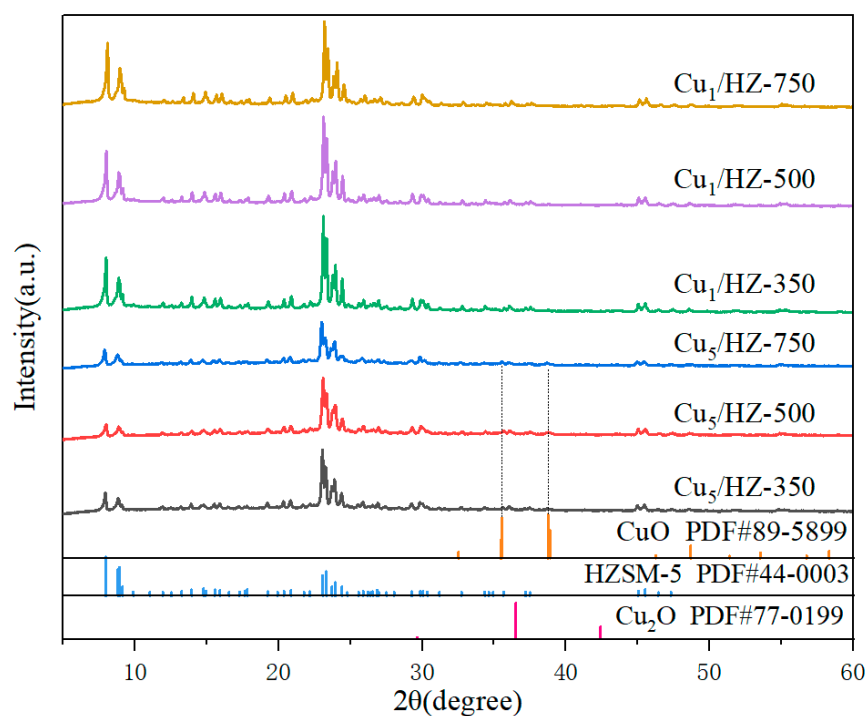


Figure 2. XRD Patterns of Cu_1/HZ and Cu_5/HZ at different calcination temperatures.

The actual loading of the catalyst was measured by ICP-OES, with the actual Cu loads for the synthesized 1 wt% and 5 wt% catalysts at 0.77 wt% and 4.30 wt%, respectively. We can further calculate the Cu/Al ratios of Cu_1/HZ and Cu_5/HZ to be 0.29 and 1.67, respectively. This indicates that Cu_1/HZ can effectively reduce the agglomeration of Cu species and improve the anti-sintering ability in the reaction process.

The N_2 adsorption/desorption of the sample before and after loading is shown in Figure 3a. According to the IUPAC classification standards, both un-loaded HZSM-5 and Cu/HZ belong to Type IV isotherms with H4 hysteresis loops produced because of capillary condensation. These structures lacked distinct adsorption saturation platforms,

indicating uneven pore structures. The H4 hysteresis loop is a typical adsorption curve for zeolites with narrow slit pores. The pore size distribution of the samples, calculated from the desorption branch of the isotherm yield using the BJH method, is shown in Figure 3b. This further suggests that the structure of the catalyst remains unchanged during the synthesis process, aligning with the XRD results. Table 1 records the specific surface area, pore volume, and pore size of the samples before and after loading. The specific surface area of the unloaded HZSM-5 was 409 m²/g with a micropore volume of 0.14 cm³/g, Cu₁/HZ-350 had a specific surface area of 390 m²/g with a micropore volume of 0.12 cm³/g, and Cu₅/HZ-350 showed a specific surface area of 337 m²/g with a micropore volume of 0.11 cm³/g. These results imply that the specific surface area and the micropore volume of the catalyst decreased after loading and diminished further as the loading amount increased. More Cu species were loaded onto the HZSM-5 surface, therefore reducing its surface area and micropore volume.

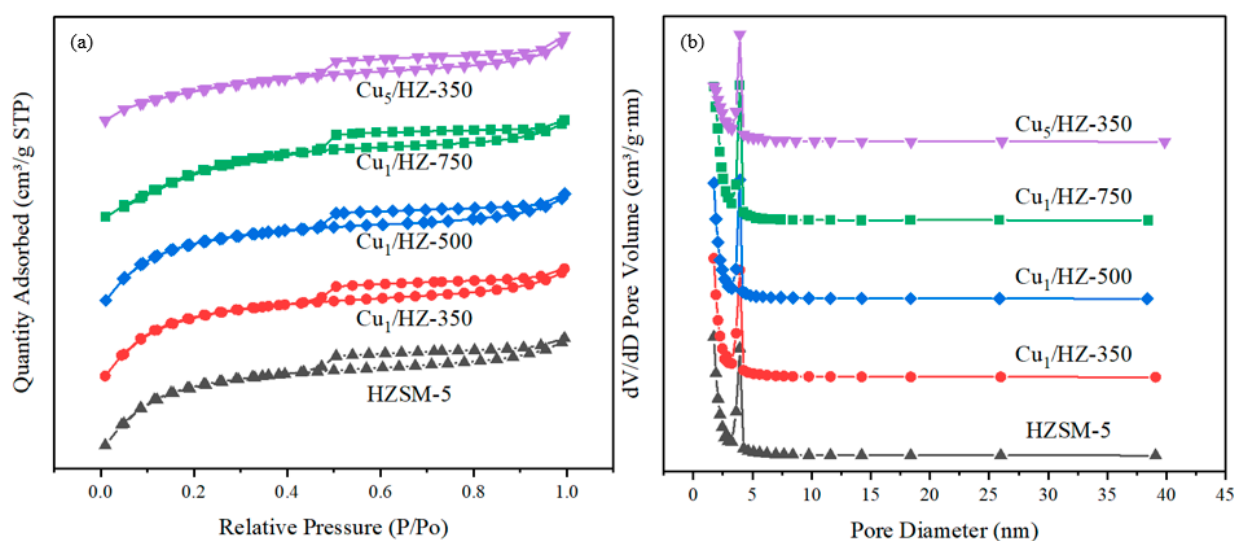


Figure 3. (a) N₂ Isothermal adsorption and desorption graph and (b) pore size distribution curves from BJH method of HZSM-5 and Cu/HZ.

Table 1. Pore properties of unloaded HZSM-5 and Cu/HZ.

Samples	S _{BET} /(m ² g ^{−1})	S _{micro} /(m ² g ^{−1})	S _{ext} /(m ² g ^{−1})	V _{total} /(cm ³ g ^{−1})	V _{micro} /(cm ³ g ^{−1})	V _{meso} /(cm ³ g ^{−1})	D _{BJH} /(nm)	D _{BET} /(nm)
HZSM-5	409.452	357.406	52.0458	0.186589	0.143210	0.043379	3.3184	1.7788
Cu ₁ /HZ-350	389.589	299.034	90.5555	0.181782	0.119855	0.061927	3.0426	1.8361
Cu ₁ /HZ-500	393.650	304.047	89.6027	0.184162	0.122046	0.062116	3.1142	1.8300
Cu ₁ /HZ-750	388.901	272.853	116.048	0.186066	0.111130	0.074936	2.8293	1.8812
Cu ₅ /HZ-350	336.721	276.283	60.4375	0.161885	0.110366	0.051519	3.6570	1.8563

The morphology and microscopic structure of the synthesized catalyst were studied by transmission electron microscopy (TEM), as shown in Figure 4. Figure 4a shows that the catalyst is made up of regular sheet structures with sizes of approximately 60 μm in length, 20 μm in width, and 20–40 nm in thickness. Figure 4 implies that Cu species exist on the surface of the body in a granular form. The particle size distribution suggests that the size of the loaded particles is primarily in the range of 3.07 nm ± 0.69 nm. This indicates that the loaded Cu oxide particles are uniformly and densely distributed on the HZSM-5 surface. The small size of the particles helps explain the lack of characteristic Cu oxide peaks in the XRD, when loaded in small amounts.

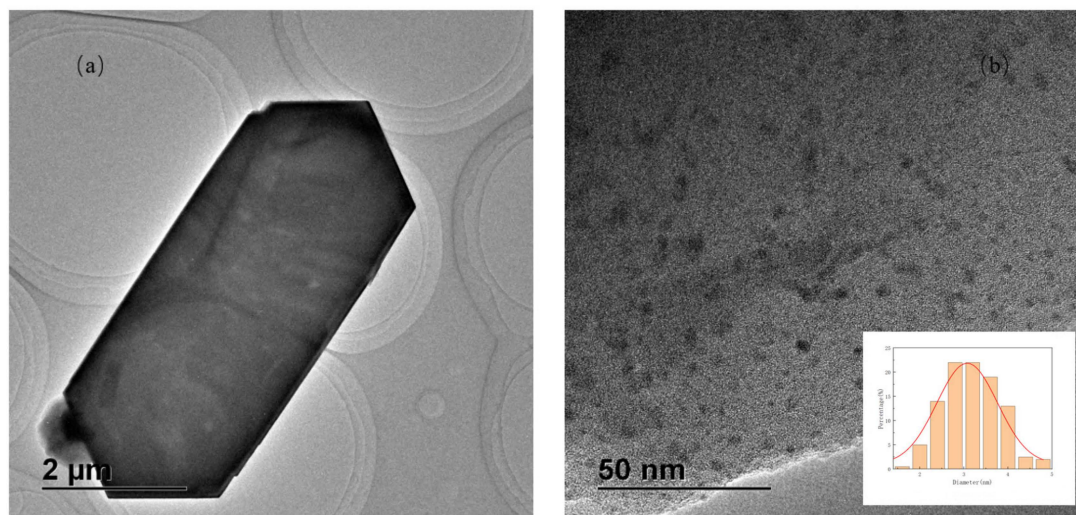


Figure 4. (a) Morphology of support in TEM image and (b) Cu_1/HZ TEM image and Cu oxide particle size distribution.

3.2. Catalytic Performance

A fixed-bed reactor was used to determine the catalytic performance of the prepared catalyst samples, as shown in Figure 5a. Among them, $\text{Cu}_1/\text{Al}_2\text{O}_3$ did not show any yield of HFPO between 180–220 °C. When SiO_2 and acid- SiO_2 served as supports, Cu_1/SiO_2 and $\text{Cu}_1/\text{acid-SiO}_2$ displayed higher activity towards HFPO at 200 °C, with HFPO yields of 6.1% and 5.7%, respectively. For $\text{Cu}/\text{HZ-500}$, we measured its reactivity at Cu loading capacities of 0.2%, 1%, and 5%, finding that the catalytic effect of $\text{Cu}_1/\text{HZ-500}$ was the best, achieving a yield of 16.3% at 180 °C. In order to confirm the catalytic performance of Cu/HZ , we also conducted a control experiment on unloaded HZSM-5 (Figure S5). The results indicate that HZSM-5 itself does not possess the catalytic activity of epoxidation for HFP. Figure 5b shows the conversion and yield of HFPO obtained at different temperature conditions using the $\text{Cu}_1/\text{HZ-500}$ catalyst. The highest yield of HFPO was achieved at around 180 °C, and increasing or decreasing the reaction temperature by 10 °C led to a significant decrease in the HFPO yield. An increase in temperature is beneficial to the forward reaction and the conversion of the reaction increases. However, too high a temperature will lead to decomposition of the generated HFPO, which makes the yield of the reaction first increase and then decrease.

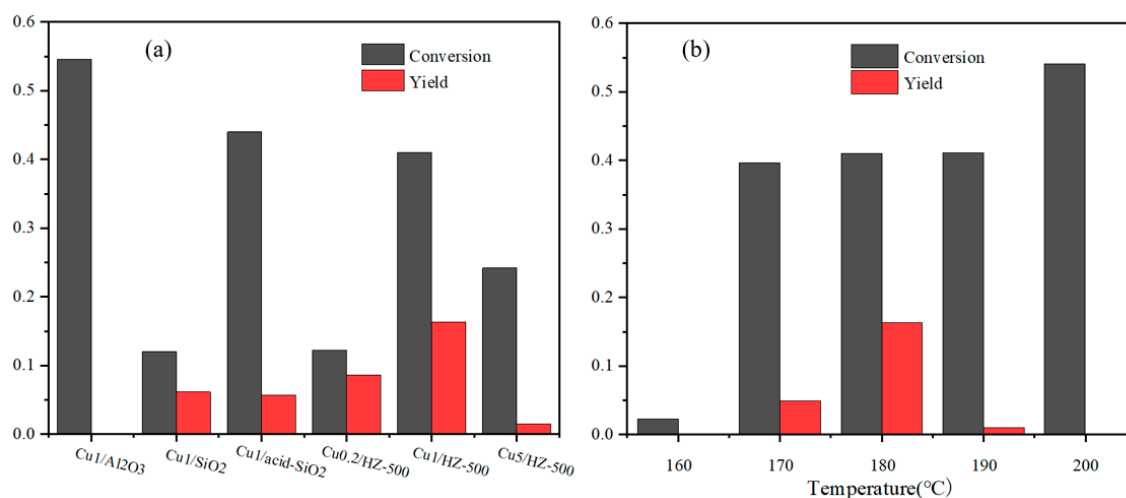


Figure 5. (a) Catalytic performance of Cu species with varying supports (detailed data in Table S1–S4). (b) Influence of reaction temperature on $\text{Cu}_1/\text{HZ-500}$.

The effects of calcination temperatures and catalyst loading amount on the catalytic performance were also studied (Table 2). The yield of HFPO using the Cu₁/HZ catalyst calcined at 350 °C reached 35.6%, significantly higher than those using the catalysts calcined at 500 °C and 750 °C with HFPO yields of 16.3% and 18.3%, respectively. In the interest of rigor, we conducted a TG test on Cu₁/HZ-350 (results can be found in Figure S16), confirming that there was no Cu(NO₃)₂ present in the catalyst. The trend of the catalytic performance of Cu₅/HZ at different calcination temperatures was similar to that of Cu₁/HZ (i.e., the catalyst calcined at 350 °C was more active than those calcined at 500 °C and 750 °C). However, the catalytic performance of Cu₁/HZ was significantly higher than that of Cu₅/HZ when both catalysts were calcined at 350 °C, suggesting a preference for lower loading capacity.

Table 2. HFP epoxidation results of catalysts at 1 wt% & 5 wt% calcined at different temperature and proportion of solitary Cu²⁺ and CuO particles.

Catalyst	Conversion/(%)	Selectivity/(%)	Yield/(%)	Cu ²⁺ /(Cu ²⁺ + CuO) ^a	Reference
Cu ₁ /HZ-350	47.6	74.8	35.6	48.75%	this work
Cu ₁ /HZ-500	41.0	39.8	16.3	31.10%	this work
Cu ₁ /HZ-750	37.5	48.9	18.3	21.87%	this work
Cu ₅ /HZ-350	43.8	61.1	26.8	43.29%	this work
Cu ₅ /HZ-500	24.2	6.20	1.50	29.24%	this work
Cu ₅ /HZ-750	48.6	1.16	0.563	33.54%	this work
10% Ag/γ-Al ₂ O ₃	14.2	40.2	5.7	—	[6]
10% Ag/γ-Al ₂ O ₃ −0.01% Cs	16.5	47.8	7.9	—	[6]
Cs-10% CuO/SiO ₂	35.5	51.4	18.2	—	[9]

^a The peak area ratio calculated in XPS spectrum.

Compared with existing related catalytic reactions, the low-temperature-calcined Cu₁/HZ also has more prominent catalytic properties. Huang et al. [6] studied the 10%Ag/γ-Al₂O₃ as a catalyst and the conversion and selectivity at 150 °C were 14.2% and 40.2%, respectively. Further, they increased the conversion and selectivity to 16.5% and 47.8%, respectively, by doping Cs. Ndlovu et al. [9] prepared Cs-modified 10%CuO/SiO₂ and obtained the highest selectivity of 51.4% at the conversion rate of 35.5%. In this work, the catalytic performance of a Cu catalyst was greatly improved by using HZSM-5 as the support without dependence on Cs doping.

3.3. XPS

The difference in catalytic performance may be attributed to different forms of Cu species on the HZSM-5 structure. To probe the chemical state of Cu species on the surface of the catalyst, X-ray photoelectron spectroscopy (XPS) was performed on the samples. Figure 6 depicts the XPS spectra of Cu₁/HZ at different calcination temperatures. As seen in Figure 6a, two main peaks appear around 933.2 eV and 953 eV for Cu₁/HZ catalysts at different calcination temperatures in the Cu2p spectra, corresponding to Cu2p_{3/2} and Cu2p_{1/2}, respectively. A satellite peak corresponding to CuO emerges between 941 and 945 eV, verifying the presence of CuO. The Cu2p_{3/2} is split into two peaks, where the peak at 933.2 eV represents agglomerated CuO nanoparticles on the catalyst surface and the other peak at around 934.5 eV corresponds to the solitary Cu²⁺ ions coordinated on the HZSM-5 surface after ion exchange [25–27]. Figure 6b also depicts two corresponding peaks split in the Cu LMM spectra, confirming the conclusions from the split peaks in 2p_{3/2}.

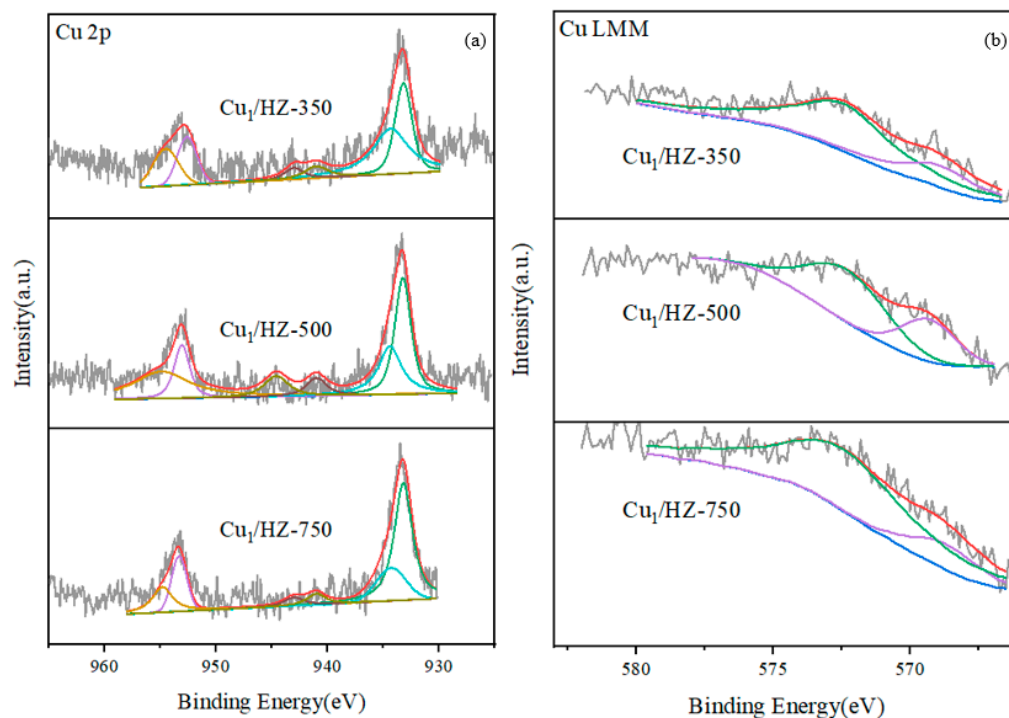


Figure 6. XPS spectra: (a) Cu 2p spectra and (b) Cu LMM spectra of Cu₁/HZ after calcination at various temperatures.

To further verify the presence of isolated Cu²⁺, EPR characterization of catalyst samples was carried out, and the results are shown in Figure S15. Since CuO, Cu⁺, and Cu⁰ are not paramagnetic, EPR spectra only respond to Cu²⁺ [28]. The results of EPR spectra show that there are isolated Cu²⁺ ions on the Cu₁/HZ-350 catalyst. Since the catalyst was tested at room temperature and the zeolite was in a fully hydrated state [29,30], the EPR spectrum of Cu²⁺ is dominated by isotropy, and the hyperfine structure of Cu²⁺ is not prominent, Cu²⁺ only partially limited to show anisotropic peaks.

The proportions of solitary Cu²⁺ and CuO on the catalyst sample surface were calculated via XPS spectra results, and Table 2 shows the results for each catalyst sample. CuO nanoparticles are predominant on the surfaces of catalyst samples. Moreover, the highest amount of solitary Cu²⁺ ions produced from ion exchange with HZSM-5 on the catalyst surface was found to be given by Cu₅/HZ-350 as compared to the conditions when calcined at 500 °C and 750 °C. The XPS spectra of Cu₅/HZ exhibited a similar trend to Cu₁/HZ, and this can be found in Figure S4.

Greiner et al. [31] reported the corrosion of Cu in the epoxidation process of ethylene, observed several oxidation states of Cu, and found that both CuO and Cu₂O have a certain degree of epoxidation activity. Wang et al. [32] studied CuO_x/SiO₂ and concluded that Cu²⁺ is the active site for epoxidation, which can be improved by alkali metals. In this work, both CuO particles and solitary Cu²⁺ ions were found in the XPS spectra. When calcination temperature was decreased, it was found that the amount of solitary Cu²⁺ ions increased and the activity of the catalyst improved at the same time. Therefore, the solitary Cu²⁺ ions on the HZSM-5 structure are probably more prone to epoxidation than CuO particles.

3.4. H₂-TPR

In the epoxidation of HFP, it is essential for catalysts to have a moderate redox property. Too-high or too-low redox properties will have consequences of complete oxidation or almost no reaction, respectively. Therefore, the redox properties of the samples—which are closely related to their catalytic performance—are illustrated through the H₂-TPR curves in Figure 7. The reduction of Cu²⁺ to Cu⁰ can occur through one or two steps. In the two-step pathway, the reduction Cu²⁺ to Cu⁺ can firstly occur at a lower temperature, and then the

reduction Cu^+ to Cu^0 can only occur at a higher temperature. The reduction peaks of the catalyst can generally be divided into two regions: the low-temperature region ($<350^\circ\text{C}$) and the high-temperature region ($>350^\circ\text{C}$). In the low-temperature region, catalyst samples with different loadings and calcination temperatures all show a pronounced reduction peak around 220°C , which is related to the reduction of isolated Cu^{2+} ions and Cu^{2+} oxy-cations to Cu^0 . The reduction peaks in the low-temperature region produced by hydrogen consumption may also include the reduction of Cu^{2+} to Cu^0 inside CuO particles. The peaks in the high-temperature region are usually associated with the reduction of Cu^+ ions, which are reduced from Cu^{2+} at a low temperature to Cu^0 [33].

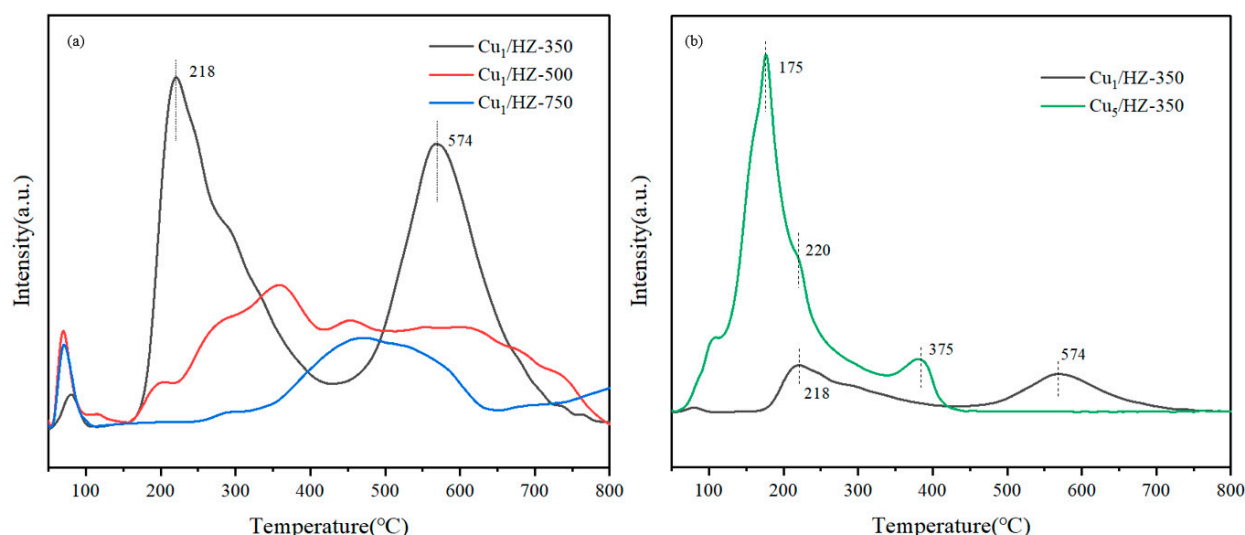


Figure 7. (a) H₂-TPR spectra of different calcination temperatures under 1 wt% loading and (b) H₂-TPR spectra of Cu₁/HZ-350 and Cu₅/HZ-350.

Figure 7a displays the reduction conditions of catalysts at different calcination temperatures. It can be observed that the Cu₁/HZ-350 catalyst has two distinct reduction peaks in the low- and high-temperature zones, corresponding to the reduction of isolated Cu^{2+} ions to Cu^+ and Cu^+ to generate Cu^0 . However, the reduction peaks in Cu₁/HZ-500 and Cu₁/HZ-750 are not as pronounced, and the peak areas representing the reduction of Cu^{2+} and Cu^+ to Cu^0 are significantly reduced. This implies that the redox performance of Cu₁/HZ-350 catalyst far exceeds those of Cu₁/HZ-500 and Cu₁/HZ-750. The Cu₁/HZ-350 possesses the highest concentration of redox sites. In Figure 7b, the reduction capabilities of Cu/HZ-350 are shown at different loadings. In Cu₅/HZ-350, the peak around 574°C , indicating Cu^+ reduction to Cu^0 , disappears. Instead, due to the increased loading, a massive reduction peak appears around 175°C , corresponding to the reduction of small CuO particles. Simultaneously, a new peak is generated at 375°C , corresponding to the reduction of bulk CuO particles to Cu^0 [34,35]. In contrast to Cu₁/HZ-350, the peak area at 218°C , representing the reduction of isolated Cu^{2+} in ion exchange positions of zeolites, does not increase significantly in Cu₅/HZ-350. This suggests that an excessive load of Cu in Cu₅/HZ-350 tends to form CuO (i.e., bulk or nanoparticles), not isolated Cu^{2+} , which is regarded to be prone to epoxidation in XPS analysis.

The same conclusion regarding the relationship between isolated Cu^{2+} and epoxidation performance can be reached through the peak position. The peak of isolated Cu^{2+} is located at a higher temperature than that of CuO nanoparticles, which means less oxidizing capacity and being prone to epoxidation.

3.5. NH₃-TPD

Although analysis of H₂-TPR can partly interpret the catalytic performance of samples, the impact of absolute amount of isolated Cu^{2+} in samples of different loading capacity

on catalytic performance is hardly explained only by characterization of H₂-TPR. Acidic properties, which are another important evaluation index of selective oxidation, are further discussed with reference to the NH₃-TPD experiment. The results are shown in Figure 8. The peaks formed from the desorption of NH₃ can be divided into weak, medium, and strong acidic sites for the samples tested, corresponding to the temperature ranges of 100–250 °C, 250–500 °C, and 500–670 °C, respectively. The low-temperature peak located at 100–150 °C is common to all samples and is generally considered to represent physical adsorption of NH₃ components on the HZSM-5 framework; these produce a peak that can desorb at lower temperatures. The peak generated around 220 °C is due to the introduction of Cu species; the newly emergent active sites adsorb NH₃, leading to desorption [36,37]. The peak around 316 °C that is only found in catalysts at a Cu loading of 5 wt% can be ascribed to the formation of CuO of larger particle size [38]. The high-temperature peak around 450 °C is generally considered to be the desorption peak produced by strong binding between B acid sites on HZSM-5 and NH₃.

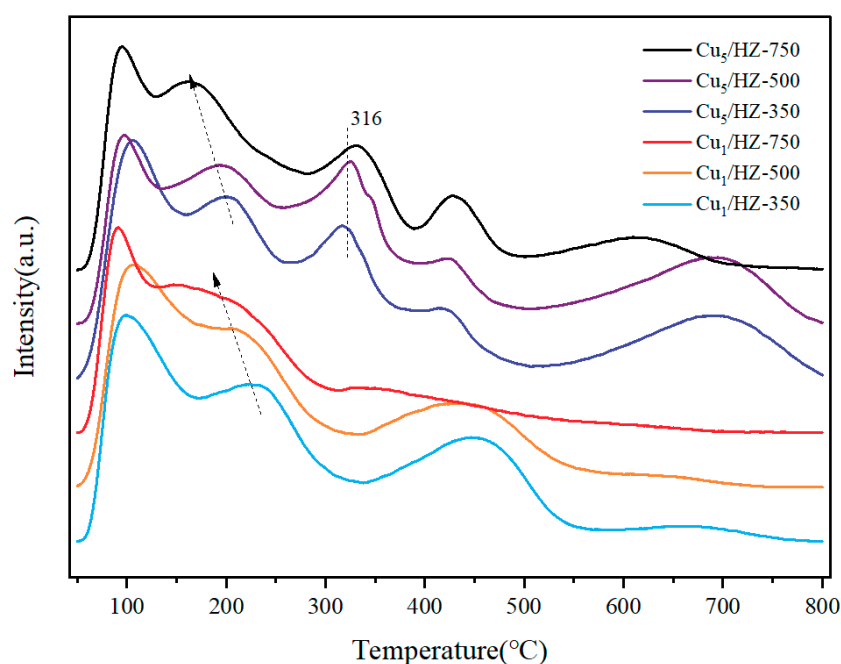


Figure 8. NH₃-TPD spectra of catalysts at different calcination temperatures and loadings.

As shown in Figure 8, at the same loading level, as calcination temperature increases, the center position of the weak acidic peak from 150 °C to 250 °C moves towards lower temperatures. This indicates that lower-temperature calcined catalysts have less interaction between Cu components and HZSM-5, which suppress the strength of acid sites and improve catalytic activity. The catalyst calcined at 350 °C has the highest total acid content. On the one hand, low-temperature calcination can preserve the original structure of ZSM-5 to the maximum extent. It prevents the zeolite structure from being destroyed, and thus reduces the acid content of the catalyst. On the other hand, low-temperature calcination can promote the break of Si-O-Al bond and increase the acidity of the zeolite. At the same time, it can avoid the reduction in acid amount due to aggregation of acid sites under high calcination temperature. Although the loading capacity increases to 5%, the total numbers of acid sites shown in Table 3 remain almost constant and do not increase to the same level as the load. This may imply that catalytic properties do not increase with load. In conjunction with the results from H₂-TPR, a larger loading tends to result in the formation of larger CuO particles adhered to the catalyst, which reduces the number of weak acid sites on the catalyst. The reduction of weak acid sites will in turn lead to a decrease in the adsorption capacity of the reactant molecules, thereby inhibiting the catalytic reactivity. It is another piece of clear evidence to explain Cu₅/HZ-350 having a higher absolute amount

of isolated Cu^{2+} but lower epoxidation performance. Among all the catalysts, $\text{Cu}_1/\text{HZ-350}$ possesses the highest concentration of weak acid sites.

Table 3. NH_3 desorption and distribution of acid sites of catalyst samples.

Sample	NH_3 Desorption (mmol/g Catalyst)	Peak Area Fraction (%)		
		Weak	Medium	Strong
$\text{Cu}_1/\text{HZ-350}$	3.977	68.6	28.2	3.3
$\text{Cu}_1/\text{HZ-500}$	3.223	68.0	29.9	2.0
$\text{Cu}_1/\text{HZ-750}$	2.352	67.1	30.5	2.4
$\text{Cu}_5/\text{HZ-350}$	3.910	57.0	26.6	16.4
$\text{Cu}_5/\text{HZ-500}$	3.622	52.0	29.6	18.4
$\text{Cu}_5/\text{HZ-750}$	3.286	55.8	35.0	9.2

3.6. Stability Experiments

The stability of $\text{Cu}_1/\text{HZ-350}$ during the reaction at 180°C was examined. As shown in Table 4, HFP underwent an epoxidation reaction on $\text{Cu}_1/\text{HZ-350}$ and the reaction was carried out for approximately 13 h. Starting from the activation of the reaction, the reaction conditions were set at 180°C , with an HFP to O_2 feed ratio of 2:1. After 7 h of the reaction, selectivity reached 77.6%. Selectivity remained almost unchanged and conversion increased further to 47.6% from 19.3% after 9 h of continuous reaction. After 13 h of the reaction, although conversion continued to increase, selectivity decreased to 42.4%.

Table 4. Conversion, selectivity, and yield of HFP to HFPO (reaction temperature 180°C , HFP: O_2 feed ratio of 2:1, pressure 0.38 MPa, total gas flow 5 sccm).

Time on Stream	Conversion/(%)	Selectivity/(%)	Yield/(%)
7 h	19.3%	77.6%	15.0%
9 h	47.6%	74.8%	35.6%
13 h	55.3%	42.4%	23.4%

3.7. Reaction Pathway

Based on the results of the catalyst performance experiments and characterization tests, we believe that the mechanism of action of the Cu/HZ catalyst system is as depicted in Figure 9. From the XPS, we can infer that isolated Cu^{2+} serves as an important site for the epoxidation of the catalyst. HFP is catalytically converted to HFPO at this active site, and the epoxidized Cu species are then reconverted to Cu^{2+} in an oxygen atmosphere. In this process, HZSM-5 is introduced as a carrier, providing the catalyst with a richer array of acid sites. This facilitates the adsorption of reactant molecules on the catalyst surface, thereby greatly enhancing the catalytic activity of the Cu-based catalyst.

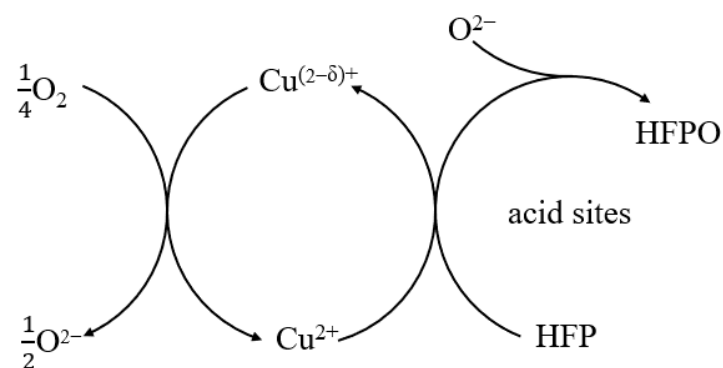


Figure 9. Cu/HZ catalyst reaction mechanism.

3.8. Causes of Inactivation

The XPS spectra were used to analyze the Cu species on the catalyst surface after the reaction, as shown in Figure 10. Compared with the catalyst before the reaction, the peak at 934.5 eV corresponding to Cu^{2+} on the HZSM-5 surface disappeared in the Cu 2p_{1/2} spectrum of the post-reaction catalyst, and the Cu 2p_{1/2} spectrum can mainly be divided into two peaks at 933.4 eV and 936.3 eV. The peak at 933.4 eV corresponds to the CuO nanoparticles on the catalyst surface, and the peak at 936.3 eV corresponds to the various active sites constituted by Cu and active oxygen on the HZSM-5 surface [39]. The formation of these active sites greatly enhanced the activity of the catalyst, causing excessive oxidation of HFP into other byproducts instead of HFPO in the reactor, which led to a considerable increase in conversion rate, while selectivity and yield dropped to zero.

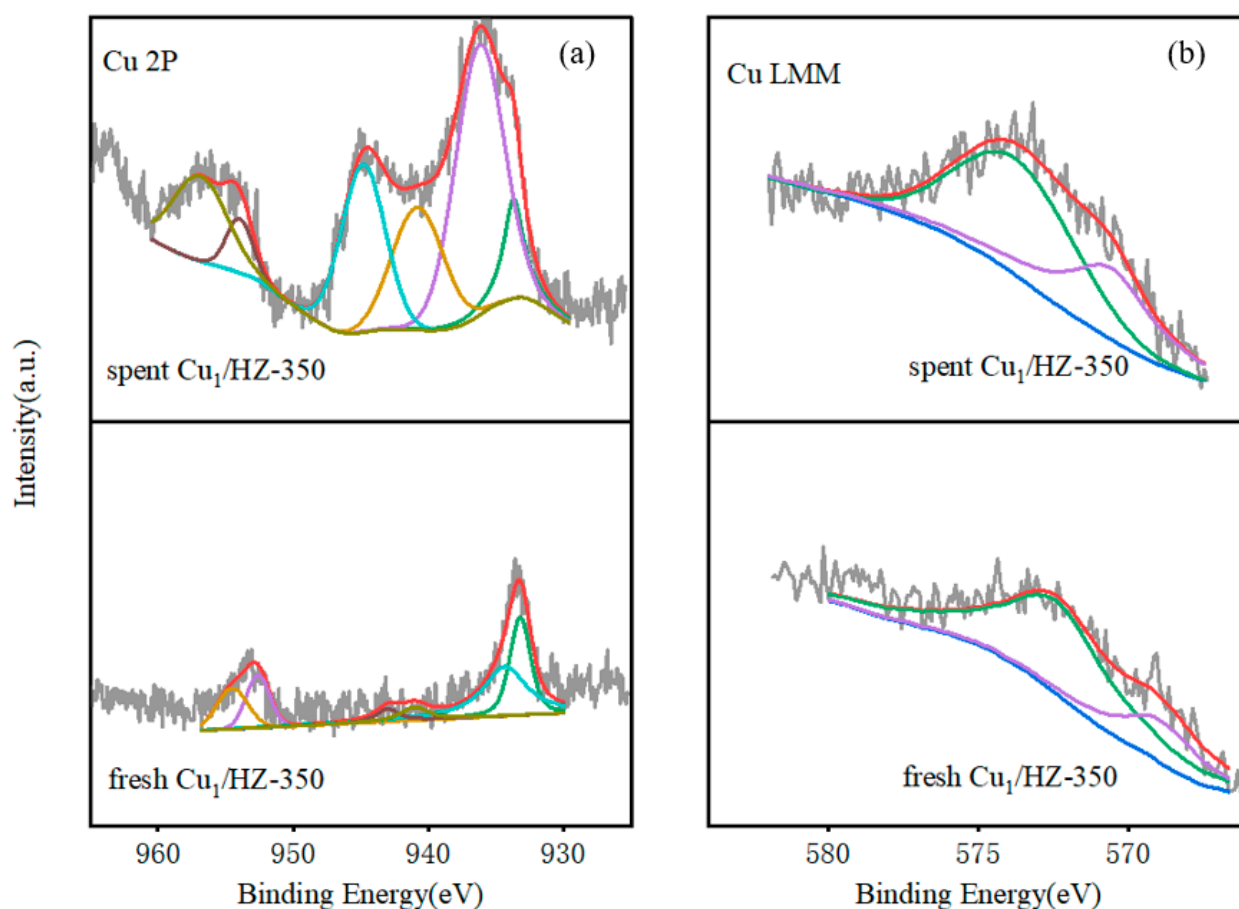


Figure 10. XPS spectra of $\text{Cu}_1/\text{HZ-350}$ before and after the reaction: (a) Cu 2p spectra and (b) Cu LMM spectra.

3.9. Thermogravimetric Analysis of Spent Catalyst

A thermogravimetric analysis was conducted on the post-reaction $\text{Cu}_1/\text{HZ-350}$, as shown in Figure 11. From the beginning of the temperature increase to 200 °C, the sample lost weight at an almost constant rate, which could be attributed to the evaporation of substances like water from the catalyst. At approximately 280 °C and 550 °C, two noticeable changes occurred in the rate of weight loss. These are very likely to correspond to the reactive substances attached to the surface of the catalyst and the combustion of carbon deposits, respectively.

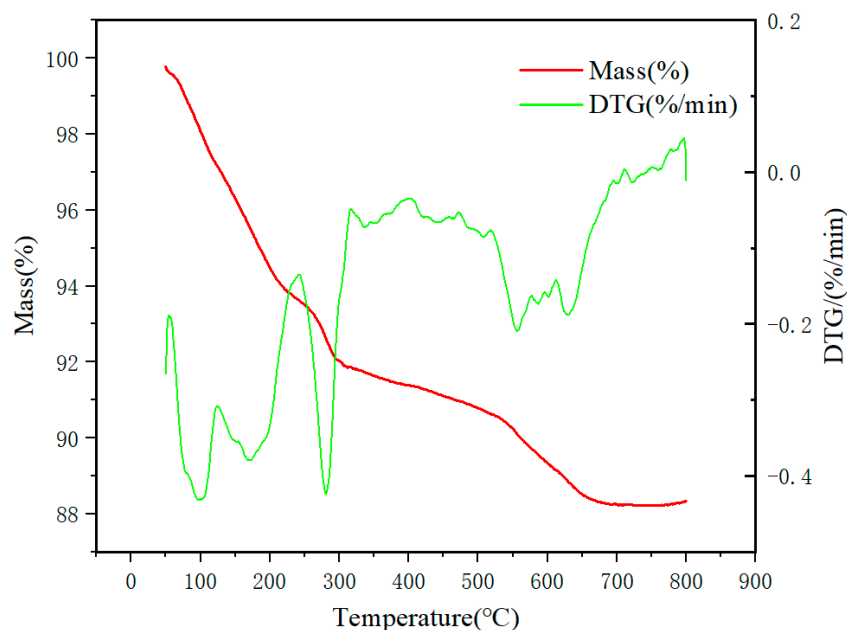


Figure 11. TGA spectrum after Cu₁/HZ-350 reaction.

Combined with XPS and TGA analysis, it is suggested that the main reason for the deactivation of Cu/HZ is the gradual transformation of Cu²⁺ into larger particles of CuO or other highly active copper compounds during the reaction. At the same time, the catalyst is also polluted by carbon accumulation and byproducts.

4. Conclusions

Direct epoxidation of HFP using molecular oxygen under gaseous conditions is a promising method of producing HFPO, wherein the combination of Cu species and HZSM-5 demonstrates superior catalytic performance over other traditional supports in the epoxidation reaction of HFP. According to the results from H₂-TPR and NH₃-TPD, this reaction advantage primarily originates from the interaction between the unique acid sites and channel structure of the HZSM-5 zeolite and the Cu species. Acid sites can improve the catalytic capacity of Cu species by increasing the adsorption of HFP. The result of XPS further shows that this interaction mainly stems from the Cu²⁺ ions generated via ion exchange with the surface of HZSM-5. Simultaneously, the sample of catalyst also preserves the inherent pore structure of HZSM-5, which can be confirmed from the results of XRD and BET. By applying catalysts prepared at various calcination temperatures with different loadings, it was found that low-temperature calcination boosts the reactivity of the catalyst, and low loading facilitates the production of HFPO. XPS and H₂-TPR analyses of the samples indicated that the main reason for these phenomena is that lower loading allows Cu²⁺ to exist in isolated forms on the HZSM-5 surface, while low-temperature calcination helps to retain isolated Cu²⁺ ions. In addition, the selectivity of catalysts to HFPO will be reduced once the isolated Cu²⁺ is converted into other forms during the reaction. Gaseous-phase epoxidation of HFP is the most promising direction for the synthesis of HFPO in the field of industrial applications. This work is expected to further improve the catalytic system involved in the reaction, and provide a new research direction for the modification of Cu-based catalysts.

Supplementary Materials: The following supporting information can be downloaded at: <https://www.mdpi.com/article/10.3390/pr12071520/s1>, Figure S1: Response factor of HFP and HFPO in gas chromatography detection; Figure S2: Correction factor of HFPO to HFP in gas chromatography detection; Figure S3: TEM images of the Cu₁/HZ-500 at different scales; Figure S4: XPS spectra (a) Cu 2p spectra (b) Cu LMM spectra of Cu₅/HZ after calcination at various temperatures.; Figures S5–S8: H₂-TPR profiles of catalyst samples; Figures S9–S14: NH₃-TPD profiles of catalyst samples; Figure S15:

EPR spectrum of Cu₁/HZ-350; Figure S16: TGA spectrum of fresh Cu₁/HZ-350; Figure S17: O 1s spectra of Cu/HZ calcination at different temperatures; Table S1: Catalytic performance of Cu₁/Al₂O₃ (HFP:O₂ feed ratio of 2:1, pressure 0.38 MPa, total gas flow 5 sccm); Table S2: Catalytic performance of Cu/SiO₂ (HFP:O₂ feed ratio of 2:1, pressure 0.38 MPa, total gas flow 5 sccm); Table S3: Catalytic performance of Cu/acid-SiO₂; Table S4: Catalytic performance of Cu₁/HZ-500 (HFP:O₂ feed ratio of 2:1, pressure 0.38 MPa, total gas flow 5 sccm). Table S5: Catalytic performance of pure HZSM-5 (HFP:O₂ feed ratio of 2:1, pressure 0.4 MPa, total gas flow 5 sccm); Tables S6–S9: Peak splitting result of H₂-TPR profiles of catalyst samples; Tables S10–S15: Peak splitting result of NH₃-TPD profiles of catalyst samples.

Author Contributions: Conceptualization, J.-M.H. and K.-J.W.; methodology, J.-M.H.; validation, J.-M.H.; investigation, J.-M.H.; writing—original draft, J.-M.H.; writing—review and editing, A.S. and K.-J.W.; supervision, J.G., C.X., A.S., K.-J.W. and C.-H.H.; project administration, J.G. and C.X.; funding acquisition, A.S., K.-J.W. and C.-H.H. All authors have read and agreed to the published version of the manuscript.

Funding: The authors are grateful for the financial support from the Zhejiang Provincial Key R&D Program (Grant No. 2022C01179) and the National Natural Science Foundation of China (Grant No. U22A20408) for this work.

Data Availability Statement: Data are contained within the article and Supplementary Materials.

Conflicts of Interest: Authors Jingning Guo and Chengmiao Xu were employed by the Zhejiang Anglikang Pharmaceutical Co., Ltd. The remaining authors declare that the research was conducted in the absence of any commercial or financial relationships that could be construed as a potential conflict of interest. Authors Jingning Guo and Chengmiao Xu had no role in the design of the study; in the collection, analyses, or interpretation of data; in the writing of the manuscript, or in the decision to publish the results.

References

- Wróblewska, A.; Milchert, E.; Meissner, E. Oxidation of Hexafluoropropylene with Oxygen to Hexafluoropropylene Oxide. *Org. Process Res. Dev.* **2010**, *14*, 272–277. [\[CrossRef\]](#)
- Eleuterio, H.S. Fluorocarbon Epoxides. U.S. Patent 3,358,003, 12 December 1967.
- Ikeda, M.; Miura, M.; Aoshima, A. Process for the Production of Hexafluoropropylene Oxide. U.S. Patent 4,902,810, 20 February 1990.
- Lawson, J.R. Two-Liquid-Phase Epoxidation of Hexafluoropropylene at Low PH. European Patent 0473398A1, 4 March 1992.
- Lee, J.C.; Yetter, R.A.; Dryer, F.L.; Tomboulides, A.G.; Orszag, S.A. Simulation and Analysis of Laminar Flow Reactors. *Combust. Sci. Technol.* **2000**, *159*, 199–212. [\[CrossRef\]](#)
- Huang, Z.; Zhang, Y.; Zhao, C.; Qin, J.; Li, H.; Xue, M.; Liu, Y. Direct gas-phase epoxidation of hexafluoropropylene with molecular oxygen using Ag catalyst. *Appl. Catal. Gen.* **2006**, *303*, 18–22. [\[CrossRef\]](#)
- Qin, J.Z.; Shan, F.F.; Chen, Y.Q. Research on Synthesis of Hexafluoropropylene. *Adv. Mater. Res.* **2013**, *773*, 445–449. [\[CrossRef\]](#)
- Oda, Y.; Uchida, K.; Morikawa, S. Preparation of Hexafluoropropylene Epoxide. Japan Patent 52,053,804, 30 April 1977.
- Ndlovu, L.; Lokhat, D.; Ramjugernath, D. Gas-phase epoxidation of Hexafluoropropene using molecular oxygen and alkali doped CuO catalyst: Mechanism and kinetics. *Catal. Commun.* **2023**, *180*, 106712. [\[CrossRef\]](#)
- Ohsaka, Y.; Tohzuka, T. Process for Preparing Hexafluoropropene Oxide. European Patent 0023014B1, 1 December 1982.
- Castellan, A.; Gregorio, G.; Padovan, M. Process for Oxidizing Fluorinated Olefins and Catalysts Useful for the Purpose. U.S. Patent 5,120,866, 9 June 1992.
- Lokhat, D.; Ramjugernath, D.; Starzak, M. Gas-phase equilibrium constants for the thermally initiated oxidation of hexafluoropropene with molecular oxygen. *J. Phys. Org. Chem.* **2015**, *28*, 460–471. [\[CrossRef\]](#)
- Lokhat, D.; Starzak, M.; Ramjugernath, D. New Insights into the Kinetics of the Gas-Phase Oxidation of Hexafluoropropene. *Prog. React. Kinet. Mech.* **2016**, *41*, 418–427. [\[CrossRef\]](#)
- Lokhat, D.; Ramjugernath, D.; Starzak, M. Kinetics of the Gas-Phase Noncatalytic Oxidation of Hexafluoropropene. *Ind. Eng. Chem. Res.* **2012**, *51*, 13961–13972. [\[CrossRef\]](#)
- Shirazi, L.; Jamshidi, E.; Ghasemi, M.R. The effect of Si/Al ratio of ZSM-5 zeolite on its morphology, acidity and crystal size. *Cryst. Res. Technol.* **2008**, *43*, 1300–1306. [\[CrossRef\]](#)
- Kim, K.-J.; Ahn, H.-G. The effect of pore structure of zeolite on the adsorption of VOCs and their desorption properties by microwave heating. *Microporous Mesoporous Mater.* **2012**, *152*, 78–83. [\[CrossRef\]](#)
- Miyake, K.; Hirota, Y.; Ono, K.; Uchida, Y.; Tanaka, S.; Nishiyama, N. Direct and selective conversion of methanol to para-xylene over Zn ion doped ZSM-5/silicalite-1 core-shell zeolite catalyst. *J. Catal.* **2016**, *342*, 63–66. [\[CrossRef\]](#)

18. Burnett, L.; Rysakova, M.; Wang, K.; González-Carballo, J.; Tooze, R.P.; García-García, F.R. Isothermal cyclic conversion of methane to methanol using copper-exchanged ZSM-5 zeolite materials under mild conditions. *Appl. Catal. Gen.* **2019**, *587*, 117272. [\[CrossRef\]](#)
19. Li, W.; Wu, G.; Hu, W.; Dang, J.; Wang, C.; Weng, X.; da Silva, I.; Manuel, P.; Yang, S.; Guan, N.; et al. Direct Propylene Epoxidation with Molecular Oxygen over Cobalt-Containing Zeolites. *J. Am. Chem. Soc.* **2022**, *144*, 4260–4268. [\[CrossRef\]](#)
20. Sugiyama, S.; Sakuwa, Y.; Ogino, T.; Sakamoto, N.; Shimoda, N.; Katoh, M.; Kimura, N. Gas-Phase Epoxidation of Propylene to Propylene Oxide on a Supported Catalyst Modified with Various Dopants. *Catalysts* **2019**, *9*, 638. [\[CrossRef\]](#)
21. Panov, G.I.; Starokon, E.V.; Parfenov, M.V.; Pirutko, L.V. Single Turnover Epoxidation of Propylene by α -Complexes (FeIII–O \bullet) α on the Surface of FeZSM-5 Zeolite. *ACS Catal.* **2016**, *6*, 3875–3879. [\[CrossRef\]](#)
22. Teržan, J.; Huš, M.; Likozar, B.; Djinović, P. Propylene Epoxidation using Molecular Oxygen over Copper- and Silver-Based Catalysts: A Review. *ACS Catal.* **2020**, *10*, 13415–13436. [\[CrossRef\]](#)
23. Pulido, A.; Concepción, P.; Boronat, M.; Corma, A. Aerobic epoxidation of propene over silver (111) and (100) facet catalysts. *J. Catal.* **2012**, *292*, 138–147. [\[CrossRef\]](#)
24. Rajendran, K.; Sharma, M.; Jaison, A.; Ankitha, M.; Tiwari, A.D.; Vinod, C.P.; Jagadeesan, D. Oxidation of ethylene by Cu/TiO₂: Reducibility of Cu²⁺ in TiO₂ as a possible descriptor of catalytic efficiency. *Catal. Sci. Technol.* **2023**, *13*, 2330–2339. [\[CrossRef\]](#)
25. Lai, S.; Meng, D.; Zhan, W.; Guo, Y.; Guo, Y.; Zhang, Z.; Lu, G. The promotional role of Ce in Cu/ZSM-5 and in situ surface reaction for selective catalytic reduction of NO_x with NH₃. *RSC Adv.* **2015**, *5*, 90235–90244. [\[CrossRef\]](#)
26. Pereda-Ayo, B.; De La Torre, U.; Illán-Gómez, M.J.; Bueno-López, A.; González-Velasco, J.R. Role of the different copper species on the activity of Cu/zeolite catalysts for SCR of NO_x with NH₃. *Appl. Catal. B Environ.* **2014**, *147*, 420–428. [\[CrossRef\]](#)
27. Espinós, J.P.; Morales, J.; Barranco, A.; Caballero, A.; Holgado, J.P.; González-Elipe, A.R. Interface Effects for Cu, CuO, and Cu₂O Deposited on SiO₂ and ZrO₂. XPS Determination of the Valence State of Copper in Cu/SiO₂ and Cu/ZrO₂ Catalysts. *J. Phys. Chem. B* **2002**, *106*, 6921–6929. [\[CrossRef\]](#)
28. Yu, T.; Wang, J.; Shen, M.; Li, W. NH₃-SCR over Cu/SAPO-34 catalysts with various acid contents and low Cu loading. *Catal. Sci. Technol.* **2013**, *3*, 3234–3241. [\[CrossRef\]](#)
29. Godiksen, A.; Vennestrom, P.N.R.; Rasmussen, S.B.; Mossin, S. Identification and Quantification of Copper Sites in Zeolites by Electron Paramagnetic Resonance Spectroscopy. *Top. Catal.* **2017**, *60*, 13–29. [\[CrossRef\]](#)
30. Giordanino, F.; Vennestrom, P.N.R.; Lundegaard, L.F.; Stappen, F.N.; Mossin, S.; Beato, P.; Bordiga, S.; Lamberti, C. Characterization of Cu-exchanged SSZ-13: A comparative FTIR, UV-Vis, and EPR study with Cu-ZSM-5 and Cu- β with similar Si/Al and Cu/Al ratios. *Dalton Trans.* **2013**, *42*, 12741–12761. [\[CrossRef\]](#)
31. Greiner, M.T.; Jones, T.E.; Johnson, B.E.; Rocha, T.C.R.; Wang, Z.J.; Armbrüster, M.; Willinger, M.; Knop-Gericke, A.; Schlögl, R. The oxidation of copper catalysts during ethylene epoxidation. *Phys. Chem. Chem. Phys.* **2015**, *17*, 25073–25089. [\[CrossRef\]](#)
32. Wang, Y.; Chu, H.; Zhu, W.; Zhang, Q. Copper-based efficient catalysts for propylene epoxidation by molecular oxygen. *Catal. Today* **2008**, *131*, 496–504. [\[CrossRef\]](#)
33. Urqujeta-González, E.A.; Martins, L.; Peguin, R.P.S.; Batista, M.S. Identification of Extra-Framework Species on Fe/ZSM-5 and Cu/ZSM-5 Catalysts Typical Microporous Molecular Sieves with Zeolitic Structure. *Mater. Res.* **2002**, *5*, 321–327. [\[CrossRef\]](#)
34. Zhou, J.; Xia, Q.-H.; Shen, S.-C.; Kawi, S.; Hidajat, K. Catalytic oxidation of pyridine on the supported copper catalysts in the presence of excess oxygen. *J. Catal.* **2004**, *225*, 128–137. [\[CrossRef\]](#)
35. Doan, T.; Dang, A.; Nguyen, D.; Vuong, T.H.; Le, M.T.; Thanh, H.P. Hybrid Cu-Fe/ZSM-5 Catalyst Prepared by Liquid Ion-Exchange for NO_x Removal by NH₃-SCR Process. *J. Chem.* **2021**, *2021*, e5552187. [\[CrossRef\]](#)
36. Leistner, K.; Xie, K.; Kumar, A.; Kamasamudram, K.; Olsson, L. Ammonia Desorption Peaks Can Be Assigned to Different Copper Sites in Cu/SSZ-13. *Catal. Lett.* **2017**, *147*, 1882–1890. [\[CrossRef\]](#)
37. Rizzotto, V.; Chen, P.; Simon, U. Mobility of NH₃-Solvated Cu^{II} Ions in Cu-SSZ-13 and Cu-ZSM-5 NH₃-SCR Catalysts: A Comparative Impedance Spectroscopy Study. *Catalysts* **2018**, *8*, 162. [\[CrossRef\]](#)
38. Xing, X.; Li, N.; Liu, D.; Cheng, J.; Hao, Z. Effect of Cu-ZSM-5 catalysts with different CuO particle size on selective catalytic oxidation of N,N-Dimethylformamide. *Front. Environ. Sci. Eng.* **2022**, *16*, 125. [\[CrossRef\]](#)
39. Guan, X.; Wang, Y.; Liu, X.; Du, H.; Guo, X.; Zhang, Z. Enhancing the Activity of Cu-MOR by Water for Oxidation of Methane to Methanol. *Catalysts* **2023**, *13*, 1066. [\[CrossRef\]](#)

Disclaimer/Publisher’s Note: The statements, opinions and data contained in all publications are solely those of the individual author(s) and contributor(s) and not of MDPI and/or the editor(s). MDPI and/or the editor(s) disclaim responsibility for any injury to people or property resulting from any ideas, methods, instructions or products referred to in the content.